geoconvention
Calgary • Canada • May 11-13 2026

Leveraging Dispersed Source Arrays for FWI optimal survey design

Joaquín Acedo, Alejandro Quiaro, Wei Zhang and Mauricio D. Sacchi

Signal Analysis and Imaging Group (SAIG), Department of Physics, University of Alberta

Summary

The Dispersed Source Arrays (DSA) concept offers a practical approach to enhancing seismic illumination and frequency content by deploying sources with complementary frequency characteristics on different spatial grids. This work examines how DSA-based acquisition influences the stability, convergence, and efficiency of full-waveform inversion (FWI) by explicitly linking the FWI gradient to the underlying acquisition parameters. Conventional acquisition lacks the multiscale information required for reliable multi-stage inversion. In contrast, DSA strategies span a broader range of wavenumbers, relaxing the requirement for a close initial model and enabling the recovery of both long- and short-wavelength components. To evaluate the impact of DSA-based acquisition on FWI performance, a standard multi-stage (MS) and a multi-stage DSA inversion workflow (MS-DSA) are compared. The numerical examples demonstrate that DSA-based strategies improve convergence behaviour, enhance the reconstruction of long- and mid-wavelength model components, and reduce computational cost. These results indicate that effective multi-stage FWI requires genuinely multiscale acquisition and that optimized DSA configurations provide a physically grounded path toward more stable and reliable inversion.

Introduction

Full-waveform inversion is a technique capable of generating high-resolution estimates of subsurface properties (e.g., P-wave and S-wave velocities, density) (Tarantola, 1984). The algorithm iteratively reduces the misfit between the observed and simulated waveforms by updating the model parameters that describe the subsurface. However, the non-linear dependence of the wavefields on model parameters and the squared least-squares misfit make the traditional FWI objective non-convex. The non-convexity of the least-squares FWI objective translates into the phenomenon of cycle skipping. When the predicted and observed waveforms differ by more than half a wavelength, the phases are misaligned, and the waveform difference enforced by the least-square misfit subtracts unintended portions of the observed and simulated data (Virieux and Operto, 2009). To mitigate these issues, many authors have proposed approaches that rely on alternative measures of the misfit distance and reformulations of the inverse problem. These approaches are commonly referred to as modified objective functions and extended inversion methods (Pladys et al., 2021; Operto et al., 2023). Modified objectives replace the traditional least-squares objective with a metric less sensitive to phase errors or amplitude inaccuracies (Luo and Schuster, 1991; Pladys et al., 2021). The extended inversion methods address non-convexity by increasing the degrees of freedom in the forward problem, allowing the inversion to "explain" data mismatches before gradually enforcing physical consistency (Symes, 2008; Operto et al., 2023). The techniques introduce additional degrees of freedom through subsurface offsets, time lags, or other extension variables such as sources. These methods are computationally intensive and can become unstable when the data contain complex wave phenomena such as multipathing or strong multiples .

A widely used strategy to improve FWI robustness practically is to perform the inversion hierarchically in a multi-stage manner (Bunks et al., 1995; Pratt, 1999). Large-scale production applications of FWI still rely on a combination of these hierarchical techniques together with travel-time or reflection-based tomography to obtain a sufficiently accurate initial model (Lambaré, 2008). Their success

depends heavily on the quality and bandwidth of the acquired data. Since conventional acquisition and processing methodologies were designed under the assumptions of traditional imaging workflows, they do not provide the low frequencies, apertures and azimuths required for inversion-based methods such as FWI. As a result, the fundamental bottleneck in FWI is the acquisition itself. In recent years, different lines of research have focused their efforts on developing new source types to extend the low end of the spectrum and new acquisition techniques to acquire higher quality data efficiently (Chelminski et al., 2019; Morgan et al., 2013; Vigh et al., 2023).

Dispersed Source Arrays (DSA) is a new acquisition concept in which arrays of sources releasing energy at different frequency bands are deployed across distinct spatial grids, replacing the traditional arrays of broadband sources (Berkhout, 2012). Each narrowband source unit in the array emits energy at a different dominant frequency, ensuring that the combined spectrum covers the temporal and spatial bandwidth required for imaging and inversion while offering several technical, environmental, and economic advantages (Caporal et al., 2018; Acedo and Sacchi, 2025).

In this paper, we investigate whether DSA can enhance the quality of the data and lead to a multi-stage algorithm for robust FWI. In particular, we demonstrate how the DSA strategies address the acquisition bottleneck by providing the frequency content and apertures necessary to enhance the low-wavenumber components of the FWI gradient, thereby mitigating or delaying cycle skipping, while also enriching the high-wavenumber information required to recover fine-scale features at the target level.

Multi-scale DSA strategy for FWI

Wu and Toksöz (1987), Sirgue and Pratt (2004), and, more recently, Abdellaziz et al. (2025) provide a physical interpretation of the gradient as a wavenumber-domain filter, along with a direct connection to the experimental setup via plane-wave analysis. Under this assumption, the gradient for a source-receiver pair is approximately

$$\nabla_{\mathbf{m}} J(\mathbf{m}) \approx \exp(i(\frac{2\pi f}{c_0})\,(\mathbf{p}_s + \mathbf{p}_r)\cdot \mathbf{x}) \tag{1}$$

where the wavenumber content of the approximate gradient is $\mathbf{k} = k_0(\mathbf{p}_s + \mathbf{p}_r)$, where $k_0 = \frac{2\pi f}{c_0}$ and $\mathbf{p}_s$ and $\mathbf{p}_r$ are the direction of the rays connecting a subsurface diffraction point to the source and receiver respectively. Following Métivier (2025), the scattering wavenumber relation describes the components injected into the model through the gradient update as

$$\|\mathbf{k}\| = \frac{2\pi f}{c_0}\cos\left(\frac{\theta}{2}\right). \tag{2}$$

Equation 2 relates the wavenumber content of the gradient with the acquisition system via the frequency f and the aperture angle θ, which is the angle between $\mathbf{p}_s$ and $\mathbf{p}_r$ and a function of the source-receiver offset. Using equation 2 for different source-receiver pairs at a given dominant frequency, Figure 1 illustrates how surface geometry and frequency content of the source can potentially affect reconstruction quality by influencing wavenumber sampling. Panel (a) corresponds to a conventional, OBN-inspired surface acquisition. Panel (b) shows the resulting wavenumber sampling. Illuminating the target from above samples only positive vertical wavenumbers. Horizontal wavenumbers are sampled symmetrically; however, large gaps appear in the low vertical wavenumber region, resulting in a blind zone. Ideally, a target-oriented FWI acquisition should maximize the area of sampled wavenumbers and distribute the samples as uniformly as possible to improve illumination. Panel (c) illustrates a DSA deployment using three sources, each positioned on a distinct spatial grid. Each source-grid matches the Nyquist requirements of its dominant frequency: low-frequency sources (red) on a coarse grid, mid-frequency sources (blue) on an intermediate grid, and high-frequency sources (green) on a denser grid. Panel (d) displays the resulting wavenumber sampling for the

DSA acquisition. The fewer low-frequency sources inject low-wavenumber components to illuminate deeper targets, allowing the algorithm to avoid cycle skipping. These regions of the wavenumber space are inaccessible to mid- and high-frequency sources. The mid- and high-frequency source grids provide denser sampling to enhance recovery of fine-scale features while bridging the mid-wavenumber gap that is typically missing in conventional surface acquisition. Consequently, DSA offers a flexible and efficient multi-scale acquisition strategy that delivers broader, denser, and more balanced wavenumber sampling, potentially mitigating cycle skipping and producing higher-resolution models.

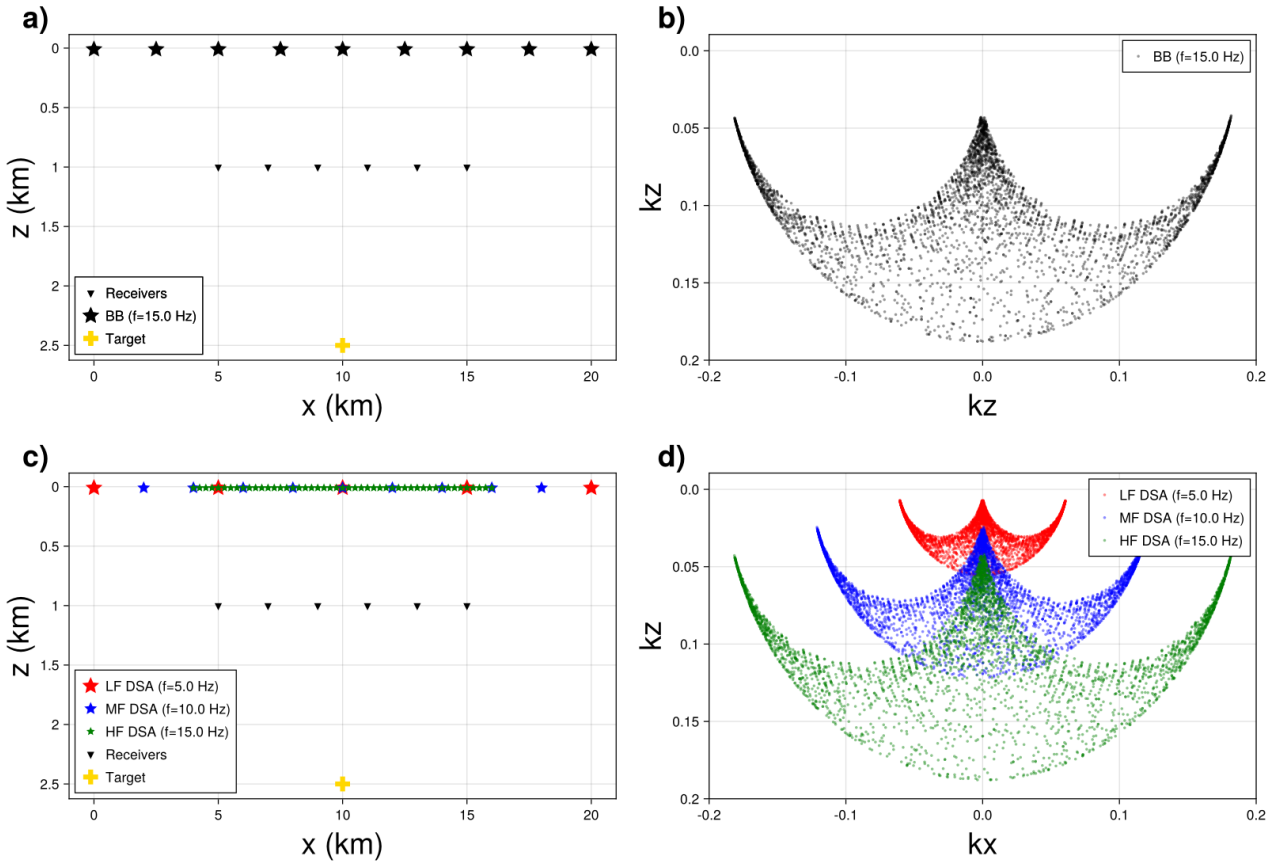


Figure 1: (a) Conventional, target-oriented OBN acquisition sketch. (b) Wavenumber sampling for conventional target-oriented acquisition. (c) Target-oriented DSA acquisition sketch. (d) Wavenumber sampling for target-oriented DSA acquisition.

Results

To evaluate the impact of DSA-based strategies on FWI, a numerical example is designed to assess inversion performance and robustness to cycle skipping and model mismatch. We compare a conventional multi-stage approach using sequential frequency bands (MS) and a multi-stage workflow based on DSA with uniformly distributed sources (MS-DSA). All inversions were performed using a nonlinear conjugate gradient (NLCG) method with line search, ensuring consistent optimization across all acquisition strategies and algorithms. The following experiments investigate how each acquisition strategy impacts convergence behaviour, reconstruction quality, and computational efficiency in multi-stage FWI. Figure 2 compares inverted models obtained with MS and MS-DSA algorithms. Panel (a) displays the thrust belt model after a smooth long-wavelength velocity bias, vertically warping of interfaces in the deeper part of the model and an elliptical lens shape heterogeneous anomaly that produces velocity disturbances of up to 5%. Panel (b) shows the initial model, obtained with a

1200 meter correlation-length Gaussian filter applied to the thrust belt model, but without the perturbations to ensure the inversion remains blind to the mismatch. Panels (c) and (d) display MS and MS-DSA inversions, respectively. The MS-DSA performs better than MS, mitigating cycle skipping

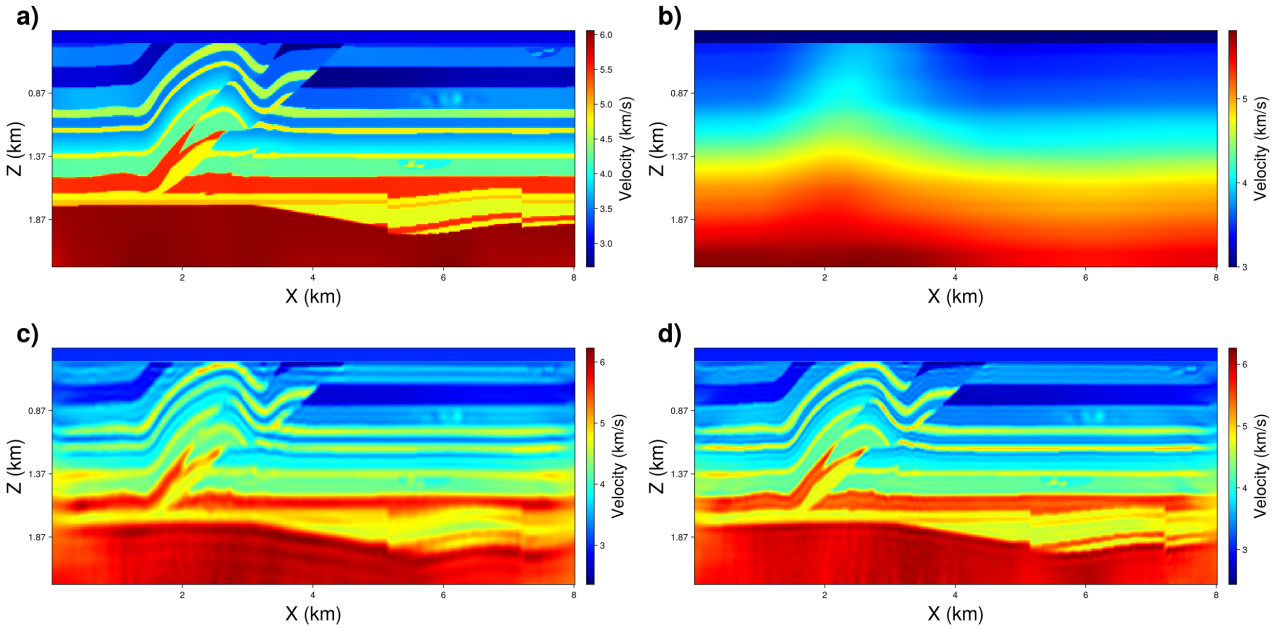


Figure 2: (a) True velocity model. (b) Initial velocity model, blind to long-wavelength bias, warping of interfaces and heterogeneous anomaly. (c) MS inversion result. (d) MS-DSA inversion result.

and reproducing band-limited versions of the structures more accurately. Figure 3 presents velocity

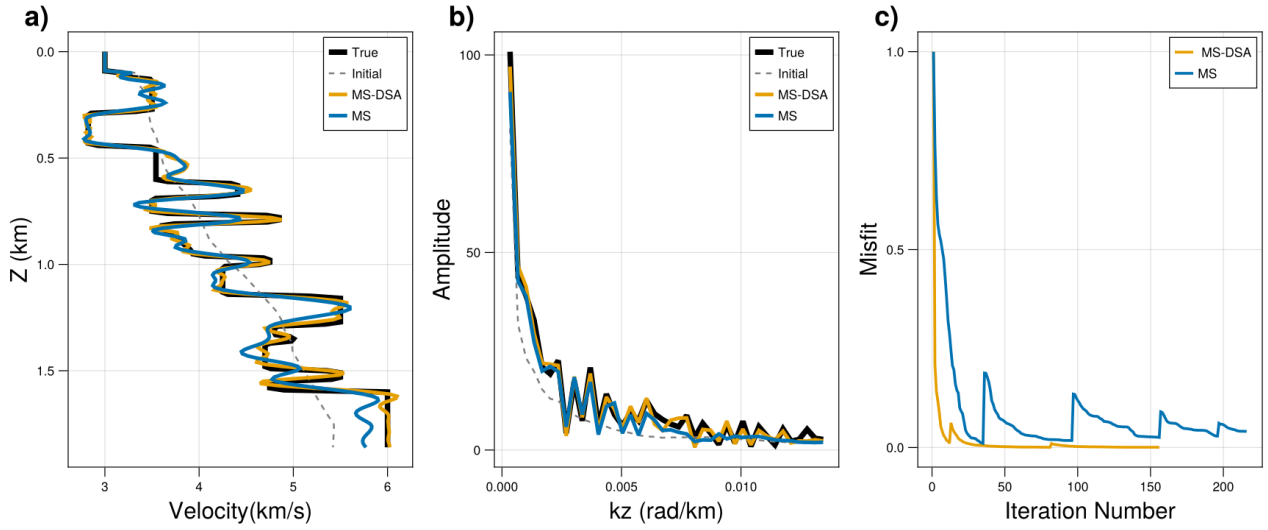


Figure 3: (a) Velocity profiles for both algorithms. (b) Wavenumber content of inverted velocity for both algorithms. (c) Misfit evolution for both algorithms.

profiles extracted at selected locations, the wavenumber content of the recovered profiles, and the misfit evolution curves for both algorithms. In this example, the MS-DSA algorithm successfully recovered both low and high wavenumbers, whereas the MS approach lacked the high wavenumber components. Panel (c) shows that the MS inversion stagnates early, consistent with cycle skipping, whereas the MS-DSA algorithm achieved a better and faster misfit reduction.

Conclusions

This study demonstrates that acquisition plays a central role in determining the stability and effectiveness of multi-scale FWI. The wavenumber-domain sampling shows that no single broadband source can populate the full range of wavenumbers required for reliable updates. Dispersed Source Arrays (DSA) address this bottleneck by injecting a broader range of frequencies and providing diverse illumination angles, thereby improving the reconstruction of the different wavelengths. The numerical experiments confirm these theoretical expectations by showing that the MS-DSA-based algorithm achieved the best results at the lowest cost. These findings lead to an alternative workflow that emphasizes the need for multi-scale acquisition for multi-stage inversion. Source diversity and optimized spatial distributions offer a practical approach to enhancing seismic data quality, thereby improving FWI robustness.

Acknowledgements

We acknowledge the Signal Analysis and Imaging Group (SAIG) sponsors at the University of Alberta for supporting the stimulating research environment that allowed the preparation of this work. Joaquin Acedo also thanks OptiSeis Solutions Ltd and the ETC Foundation for their interest and financial support in developing this work. This publication was prepared using `SeismicJulia`, a package for reproducible seismic processing, imaging, and inversion by SAIG (https://github.com/SeismicJulia).

References

Abdellaziz, A., R. Brossier, L. Métivier, and É. Oudet, 2025, Optimal experimental design for full waveform inversion using a wavenumber sampling criterion—part 1: 2-d to methodological development: Geophysical Journal International, **240**, 1429–1459.

Acedo, J., and M. D. Sacchi, 2025, Multisource wavefield reconstruction via nonuniform dispersed source arrays: Geophysics, **90**, P57–P72.

Berkhout, A., 2012, Blended acquisition with dispersed source arrays: Geophysics, **77**, A19–A23.

Bunks, C., F. M. Saleck, S. Zaleski, and G. Chavent, 1995, Multiscale seismic waveform inversion: Geophysics, **60**, 1457–1473.

Caporal, M., G. Blacquière, and M. Davydenko, 2018, Broadband imaging via direct inversion of blended dispersed source array data: Geophysical Prospecting, **66**, 942–953.

Chelminski, S., L. M. Watson, and S. Ronen, 2019, Research note: Low-frequency pneumatic seismic sources: Geophysical Prospecting, **67**, 1547–1556.

Lambaré, G., 2008, Stereotomography: Geophysics, **73**, VE25–VE34.

Luo, Y., and G. T. Schuster, 1991, Wave-equation traveltime inversion: Geophysics, **56**, 645–653.

Morgan, J., M. Warner, R. Bell, J. Ashley, D. Barnes, R. Little, K. Roele, and C. Jones, 2013, Next-generation seismic experiments: wide-angle, multi-azimuth, three-dimensional, full-waveform inversion: Geophysical Journal International, **195**, 1657–1678.

Métivier, L., 2025, High resolution geophysical imaging using full waveform modeling and inversion: Lecture notes. (Course material).

Operto, S., A. Gholami, H. Aghamiry, G. Guo, S. Beller, K. Aghazade, F. Mamfoumbi, L. Combe, and A. Ribodetti, 2023, Extending the search space of full-waveform inversion beyond the single-scattering born approximation: A tutorial review: Geophysics, **88**, R671–R702.

Pladys, A., R. Brossier, Y. Li, and L. Métivier, 2021, On cycle-skipping and misfit function modification for full-wave inversion: Comparison of five recent approaches: Geophysics, **86**, R563–R587.

Pratt, R. G., 1999, Seismic waveform inversion in the frequency domain, part 1: Theory and verification in a physical scale model: Geophysics, **64**, 888–901.

Sirgue, L., and R. G. Pratt, 2004, Efficient waveform inversion and imaging: A strategy for selecting temporal frequencies: Geophysics, **69**, 231–248.

Symes, W. W., 2008, Migration velocity analysis and waveform inversion: Geophysical prospecting, **56**, 765–790.

Tarantola, A., 1984, Inversion of seismic reflection data in the acoustic approximation: Geophysics, **49**, 1259–1266.

Vigh, D., X. Cheng, J. Xu, and K. Jiao, 2023, Forge ahead in acquisition and model building via full-waveform inversion: Gulf of mexico case study: Geophysics, **88**, B285–B295.

Virieux, J., and S. Operto, 2009, An overview of full-waveform inversion in exploration geophysics: Geophysics, **74**, WCC1–WCC26.

Wu, R.-S., and M. N. Toksöz, 1987, Diffraction tomography and multisource holography applied to seismic imaging: Geophysics, **52**, 11–25.